Disentangling heritability and plasticity effects on *Populus fremontii* leaf reflectance across a temperature gradient

Seeley, M. M.[1*†]; Thomson, E.[2]*; Allan, G. J[3]; Wiebe, B. C.[4]; Whitham, T. G. [3]; Hultine, K. R.[5]; Cooper, H. F.[3,6]; Asner, G. P.[1]; Doughty, C.E.[4]

1. Center for Global Discovery and Conservation Science, Arizona State University, Hilo, HI 96706
2. School of Geography & the Environment, University of Oxford, Oxford, UK
3. Department of Biological Sciences and Center for Adaptable Western Landscapes, Northern Arizona University, Flagstaff, AZ 86011, USA
4. School of Informatics, Computing, and Cyber Systems, Northern Arizona University, Flagstaff, AZ, USA
5. Department of Research, Conservation and Collections, Desert Botanical Garden, 1201 North Galvin Parkway, Phoenix, AZ 85008, USA
6. Center for Adaptable Western Landscapes, Northern Arizona University, Flagstaff, AZ 86011, USA

*Equal first authors

†Corresponding author; mseeley1@asu.edu

ORCID iDs

Megan M. Seeley https://orcid.org/0000-0003-1945-1162

Eleanor Thomson https://orcid.org/0000-0003-1670-8970

Gerard J. Allan https://orcid.org/0000-0002-8007-4784

Benjamin C. Wiebe https://orcid.org/0000-0002-9325-1540

Thomas G. Whitham https://orcid.org/0000-0002-1262-4342

Kevin Hultine https://orcid.org/0000-0001-9747-6037

Hillary F. Cooper https://orcid.org/0000-0003-2634-1404

Gregory P. Asner https://orcid.org/0000-0001-7893-6421

Christopher E. Doughty https://orcid.org/0000-0003-3985-7960

Keywords

Populus fremontii, cottonwood, spectroscopy, hyperspectral, plasticity, heritability, genotypic variation, extreme temperatures; forest; tree; heat

Abstract

Globally, vegetation biodiversity is expected to decline as the rate of plant adaptation struggles to keep pace with rising temperatures. To support conservation efforts through remote sensing, we disentangled the nested effects of genetic and environmental influences on reflectance spectra, leveraging spectroscopy to assess plant adaptations to temperature. Specifically, we quantified the relative effect of plasticity and heritability on *Populus fremontii* (Fremont cottonwood) leaf reflectance using clonal replicates propagated from 16 populations and grown across three common gardens spanning a mean annual temperature gradient representing the thermal range of *P. fremontii*. We used variance partitioning to decompose phenotypic variation expressed in the leaf spectra into genotypic and environmental components to estimate broad-sense heritability. Heritability was strongly expressed in the spectral red edge (~680-750nm) and shortwave infrared (~1400-3000nm), though the heritability peak in the red edge was sensitive to extreme temperatures. By comparing distances of group centroids in principal component space, we determined that *P. fremontii* intraspecific spectral variation was shaped by the interaction between common garden site conditions and source population. Support vector machine models indicated pronounced environmental influence on spectral variation, as *P. fremontii* source population and garden location were classified at 71.8% and 92.6% accuracy, respectively. These findings emphasize the utility of reflectance data in separating genetic and environmental influences on plant phenotypes, offering a pathway to scale these insights across broader landscapes and aid in the conservation and management of vulnerable ecosystems in a warming climate.

Introduction

Globally, forests are threatened by climate change through increasing temperatures and drought, leading to widespread tree mortalities (Allen et al., 2010). Many regions have already experienced declines in biodiversity, and these declines are predicted to accelerate (Pimm et al., 2014). Remote sensing, specifically imaging spectroscopy, has emerged as a powerful tool for addressing these challenges, offering insights into biodiversity, species distributions, and ecosystem health at the landscape scale (Rose et al., 2015; Seeley & Asner, 2021; Turner et al., 2003). For example, forest conservation applications of imaging spectroscopy include accurate, high-resolution species mapping (e.g. Balzotti et al., 2020; Seeley et al., 2023c), large-scale biodiversity estimations to inform and support protected area establishment (Asner et al., 2017; Féret & Asner, 2014), and forest physiological and chemical monitoring (Brodrick & Asner, 2017; Roberts et al., 2003; Weingarten et al., 2021). Imaging spectroscopy can also be used to explore plastic responses to changing environmental conditions and heritable, intraspecific trait variation that enables species to adapt to changing climates and novel conditions (Czyż et al., 2020; Seeley & Asner, 2023; Wang et al., 2022).

Previous research has successfully linked leaf and canopy spectra to both environmental and genetic factors. For example, visible through shortwave-infrared (VSWIR) reflectance data have been used to track environmental responses, such as changes in leaf traits due to stress or climatic variation (Czyż et al., 2020; Seeley & Asner, 2023). It has also been used to distinguish individuals within a species based on their genotype (Blonder et al., 2020; Cavender-Bares et al., 2016; Seeley et al., 2023b). However, many of these studies focus on either genetic or environmental influences, with limited attention to how environmental sensitivity of plant traits, and therefore spectra, can affect phylogenetic studies or how genetic differences in plasticity

influence spectral responses to environmental adaptation. Together, these considerations have the potential to reveal insights into how plants adapt and respond to changing conditions.

We used a common garden experiment to assess plastic and genotypically constrained responses of leaf reflectance spectra in *Populus fremontii* (Fremont cottonwood). *P. fremontii* inhabits riparian zones in the southwest United States and Mexico and is recognized as one of the most important foundation species in these regions (Ellison et al., 2005; Whitham et al., 2006) due to its ability to structure communities across multiple trophic levels, drive ecosystem processes, and influence biodiversity via genotypically based functional trait variation (Ferrier et al., 2012; K. C. Grady et al., 2013). Despite active planting projects, the areal extent of *P. fremontii* has declined dramatically over the last century due to water extraction, competition with invasive species, and climate change (Braatne et al., 1996; Shafroth et al., 1995; Stromberg, 1998). To support management decisions for *P. fremontii* and protect riparian ecosystems vulnerable to climate change, we attempted to link leaf-level spectral data to temperature adaptations. By deconstructing VSWIR spectra into heritable and plastic components, we aimed to map and monitor *P. fremontii* responses and tolerance to changing climate conditions and to derive a method for quantifying the heritable resilience (intraspecific variation in plant traits that could result in greater ecosystem resilience; Turner, 2023; Vahsen et al., 2023) of *P. fremontii* populations to extreme temperatures at large spatial scales.

Heritability is a statistic that estimates the degree of variation in a phenotypic trait that is due to genetic variation between individuals of a population. Measuring heritability in plant traits has long been a practice in selective breeding programs searching for heritable traits to maximize yield and quality (Bradshaw, 2017). Broad-sense heritability is defined as $H^2=v(G)/v(E)$, where v(G) is the proportion of genetic variance and v(E) is the proportion of environmental variation,

typically quantified using clonal replicates (Hühn, 1975). Thus, broad-sense heritability can vary according to the amount of environmental variation experienced by individuals. As spectroscopy integrates a vast array of leaf traits in its analyses and is a better predictor of plant and ecosystem function than a subset of foliar traits (Yan et al., 2021), quantifying heritability across the reflectance spectrum may yield novel insights into genetic versus environmental controls on leaf spectra, which are linked to functional traits, and reveal parts of the spectrum useful for retrieving phylogenetic information.

By examining *P. fremontii* leaf reflectance across three common gardens spanning the thermal range of *P. fremontii*, we sought to disentangle the genetic and environmental factors shaping its adaptive capacity to varying temperatures. Specifically, our objectives were to: 1) quantify the relative contributions of genetics (source population) and environmental influences (common garden site) to intraspecific spectral variation, 2) explore adaptations to environmental extremes by analyzing reflectance spectra, with a focus on phenotypic plasticity and genetic differentiation under extreme temperatures, and 3) identify conserved and variable regions across the VSWIR spectra of *P. fremontii* across the common gardens.

Materials and Methods

Study Sites

Three common garden sites were established across the thermal range of *P. fremontii* in 2014. Two were located at the thermal edges of the *P. fremontii* temperature range (Yuma, Arizona: 22.8°C and Canyonlands, Utah: 10.7°C), and one garden was in the middle of this range (Agua Fria, Arizona: 17.2°C; Figure 1; Table 1). As Yuma experiences extreme temperatures where ambient temperatures could exceed the critical temperature at which

Photosystem II is disrupted (t_{crit}) (Moran et al., 2023), we were able to assess the responses of leaf spectra when trees experienced air temperatures approaching and surpassing their critical leaf temperature thresholds (Hultine et al., 2020; Moran et al., 2023).

Each garden hosted cuttings from sixteen geographically separate (minimum 13.5 km) *P. fremontii* populations across Arizona spanning 12.2ºC Mean Annual Temperature. From each cutting, clonal replicates were propagated in a greenhouse. 32 clonal replicates of each cutting were planted in each common garden, across 4 stratified random blocks to minimize the effect of within-garden variation on a population. Each common garden hosted 16 wild populations of *P. fremontii*, eight genotypes (cuttings) from each population, and 32 clonal replicates from each genotype, resulting in 4096 *P. fremontii* saplings per garden. Trees at the common gardens were routinely watered to facilitate establishment in the arid southwest. A detailed description of the common garden establishment can be found in Cooper et al. (2019, 2022).

P. fremontii in the common gardens represented two distinct ecotypes (Blasini et al., 2021; (Bothwell et al., 2023; Ikeda et al., 2017). Three source populations were located on the Mogollon Rim in the Colorado Plateau and are part of the Utah High Plateau/Mogollon Rim ecotype (Blasini et al., 2021; Ikeda et al., 2017). The remaining thirteen populations represented the environmental range of the Sonoran Desert. Two secondary ecotypes (northern and southern) within the primary Sonoran Desert ecotype were represented (Bothwell et al., 2023). The larger, northern clade includes nine source populations and is referred to as the main Sonoran Desert cluster, while the southeast (SE) Sonoran Desert cluster includes three populations in the southeastern portion of Arizona. Lastly, one population (KWF) did not fall into either Sonoran Desert cluster.

Leaf Measurements

We measured leaf reflectance spectra from trees at the three common gardens in May 2018, four years after the saplings had been planted. Due to the differential survivorship of the saplings, the number of trees sampled from each population at each garden varied (0-52; Table S1). Three leaves were collected from each tree, and, where possible, leaves were harvested from different branches. Only full-expanded, sunlit adult leaves were chosen. Leaves were harvested by hand and transported in a cool box to the nearby field station for processing the same day.

Spectral measurements were collected using a leaf clip and Analytical Spectra Devices (ASD) field spectrometer from 350 to 2500 nm at 1-nm intervals (Analytical Spectra Devices Inc., Boulder, CO, USA). Three measurements were taken on the adaxial surface of each leaf in the center and averaged. The spectrometer was optimized using a white reference taken after every three leaves. To minimize noise, wavelengths with a low signal-to-noise ratio were removed (<400 nm and >2450 nm). Brightness normalization was applied to all spectral measurements to minimize variation not related to leaf chemistry and structure (Kruse et al., 1993; Myneni et al., 1989).

Leaf trait measurements and analyses

Following spectral measurements, leaves were scanned using a digital scanner (Canon LiDE 110) to determine their area, oven dried at 70 ◦C for three days and weighed for their dry mass. Leaf mass per area (LMA) was calculated by dividing the leaf's dry mass (g) by its fresh one-sided area (m^2).

The degree of stress experienced by each tree was estimated by calculating the photochemical reflectance index (PRI) (Equation 1; Thénot et al., 2002).

Equation 1: $$PRI = \frac{\rho_{531} - \rho_{570}}{\rho_{531} + \rho_{570}}$$

PRI quantifies the normalized difference between ρ_{531}, the reflectance at 531 nm, and ρ_{570}, that at 570 nm, to capture xanthophyll pigment content and epoxidation state in leaves. The quantity and epoxidation state of xanthophyll pigments in leaves respond to plant stress and are an indicator of thermal tolerance and photosynthetic efficiency (Gamon et al., 1992). PRI has been used as an indicator of plant stress at both the leaf and airborne levels (Buddenbaum et al., 2015; Hernández-Clemente et al., 2011; Rossini et al., 2013).

We next calculated solar-weighted reflectance, or albedo, for the visible (400-700nm) and near-infrared (NIR)-shortwave infrared (SWIR; 700-2500nm). Reflectance spectra (not brightness normalized) were weighted by the solar irradiance spectrum (ASTM G173-03 Reference Spectra derived from SMARTS version 2.9; Gueymard, 2004) to calculate broadband albedo (Bartlett et al., 2011) according to Equation 2, where λ represents each wavelength:

Equation 2: $$Albedo \approx \frac{\sum_{i=min}^{max} Reflectance\,(\lambda_i) \cdot Incident\ Irradiance\,(\lambda_i) \cdot \delta\lambda}{\sum_{i=min}^{max} Incident\ Irradiance\,(\lambda_i) \cdot \delta\lambda}$$

To determine whether the common garden sites induced changes in leaf traits, a Tukey-Kramer multiple comparison test from the scipy python package (Virtanen et al., 2020) was applied to the albedo, PRI, and LMA data.

Phenotypic variation in leaf spectra

To explore phenotypic variation in leaf spectra, we first visualized spectral variation across the three common gardens. Mean source population spectra at each common garden site were plotted and colored according to site. Spectral differences between the same populations at different common garden sites were further visualized using principal component analysis (PCA). PCA reduces the dimensionality of the spectral data from over 2000 dimensions to a

handful of dimensions that explain the primary spectral variation across multiple channels (Boardman & Green, 2000; Green & Boardman, 2000; Thompson et al., 2017). We randomly selected 104 spectra from among the five populations that were represented in all three common gardens (CLF, KWF, BCE, PSA, and SCT). Using scikit-learn (Pedregosa et al., 2011), we applied PCA to spectra data, plotting the first two principal components (PC) along the x and y axes. As higher PC are often important in spectroscopy applications for discriminating differences in surface chemistry and other traits (Dai et al., 2022; Thompson et al., 2017), we further visualized spectral differences across ecotypes and common gardens in the first 20 PCs. As the effect of extreme heat at Yuma was obvious in the first two PCs (Figure 3), this second analysis included spectral data from only Agua Fria and Canyonlands. Data were grouped by ecotype (Colorado Plateau, Sonoran Desert Main, and Sonoran Desert Southeast (SE)) and garden, randomly selecting spectra from 40 trees from each ecotype-garden combination. We then calculated the centroids (group mean) of each ecotype-garden combination in the first 20 PCs and measured the Euclidean distances between these centroids. Distances were then projected into 2D space using multidimensional scaling (MDS), following the approach of Seeley et al. (2023c).

Decomposing genotypic and environmental variation across the spectra and estimating broad-sense heritability

To quantify the relative effects of environmental versus genotypic variation across the VSWIR, we used variance partitioning to decompose observed variance at each wavelength into the relative contribution of site, ecotype, population, genotype, or clone. All sampled data was used across all common garden sites. Following the method of Asner et al. (2014) and Fyllas et

al. (2009), variance partitioning was calculated using a linear mixed-effects model for each wavelength across the VSWIR using the lme4 *R* package (Bates et al., 2015). The model was fitted using Residual Maximum Likelihood (REML). All effects were treated as random. Common garden site was included as a crossed random effect, while clones were nested within genotypes, which were nested within populations, which were nested within ecotype. The total spectral variance about the mean for a given wavelength was, therefore, quantitatively parsed into the variance explained by site ($\sigma 2_s$), ecotype ($\sigma 2_e$), populations within ecotype ($\sigma 2_p$), genotypes within populations ($\sigma 2_g$), clones within genotypes ($\sigma 2_c$) and residual variance ($\sigma 2_r$) according to Equation 3:

$$\text{Equation 3:} \quad \sigma 2_{total} = \sigma 2_s + \sigma 2_e + \sigma 2_p + \sigma 2_g + \sigma 2_c + \sigma 2_r$$

We next calculated broad-sense heritability across the VSWIR. Heritability at each wavelength was calculated using the classic broad sense heritability equation ($H^2 = V_G/V_P$), where V_G is genotypic variation, and V_P is total variation ($V_G + V_E$). Variance explained by ecotypes, populations, and genotypes is categorized as genotypic variance (V_G), as the genetic material within these groups differs. Variance explained by site and clones, as well as residual variance, is categorized as environmental variation (V_E), or spectral plasticity, as the genetic material within these groups is identical, so any observed differences in the spectra must be due to environment or measurement error. Broad-sense heritability was plotted across the VSWIR spectrum. This analysis was applied first to data from all three sites and then to data from Canyonlands and Agua Fria alone. To obtain confidence intervals for H^2, we employed a nonparametric bootstrap approach. Bootstrapping, a method commonly used for obtaining uncertainty estimates for heritability (Schweiger et al., 2016), involves resampling the dataset with replacement and recalculating the variance with each subsampled dataset. We performed

1000 iterations for each wavelength, sampling 31 spectra from each common garden x ecotype combination, resulting in n=279 for each iteration. Mean H^2 of the 1000 iterations were presented along with the 95% confidence interval calculated from the bootstrapped estimates.

Using leaf spectra to predict genotypic and environmental information

To explore whether leaf spectra could be used to extract both genotypic and environmental information, we used a support vector machine (SVM) to predict *P. fremontii* source population (genotypic variation) and garden location (environmental variation). SVMs efficiently handle highly dimensional datasets by creating decision boundaries in n-dimensional space that maximize the distance between class boundaries and sample points (Melgani & Bruzzone, 2004). SVMs tend to outperform other machine learning algorithms such as random forest for species and genotype classifications when applied to spectroscopy data (e.g. Dalponte et al., 2012). For each radial basis function kernel SVM, we optimized hyperparameter selection through a cross-validation grid search implemented in python with the scikit-learn package (Pedregosa et al., 2011). As with the PCA analyses, 104 samples from each garden were randomly selected from the same five source populations (CLF, KWF, BCE, PSA, and SCT). For all models, data were divided into training/test datasets using a 70/30 stratified random split.

To assess the generalizability of models in unseen and extreme environments in predicting genotypic information, we trained three additional SVM models. Each model was trained to predict source population using *P. fremontii* spectra from two of the gardens and tested on unseen spectra from the third garden. A different garden was withheld each time. This allowed us to compare the applicability of the model in extreme environments and assess how well the model can extrapolate outside of its training data.

Results

VSWIR leaf spectra responded to common garden treatment, particularly at Yuma, which represents the upper end of the cottonwood thermal range. Brightness-normalized reflectance of all populations at the Yuma site diverged from that at both Canyonlands and Agua Fria (Figures 2a & 3a). Albedo in both the visible and NIR-SWIR differed across the common gardens ($p<0.05$) and was highest at Yuma. In the visible, albedo was lowest at Canyonlands, and in the NIR-SWIR, albedo was lowest at Agua Fria. PRI, the plant stress indicator where more negative values indicate greater plant stress, was 0.018 for both Agua Fria and Canyonlands when averaged across populations. At Yuma, mean PRI decreased to -0.011 (Figure 2b). While this decrease was significant according to the Tukey-Kramer test ($p<0.05$), PRI did not vary significantly between source populations.

LMA, an important driver of spectral variation, was highest in the Yuma common garden and lowest in Canyonlands ($p<0.05$; Figure 2b). Mean LMA across all populations at Canyonlands was 72.9 g/m^2 with a standard deviation of 10.2 g/m^2. At Agua Fria, the mean LMA was 88.1 g/m^2, though it was the most variable with a standard deviation of 19.1 g/m^2. Yuma exhibited the highest LMA at 108.4 g/m^2 and a standard deviation of 11.2 g/m^2.

In PC space, spectra differed across the common gardens and among the ecotypes (Figure 3). The first two PC of spectra from all common gardens explained 57.8 and 35.3% of the variance, respectively. These components primarily separated Yuma spectra from those at Canyonlands and Agua Fria (Figure 3a). When comparing spectra from different ecotypes at Canyonlands and Agua Fria, the Colorado Plateau ecotype separated from both Sonoran Desert

ecotypes regardless of common garden in the first 20 PCs. Within the Sonoran Desert ecotypes (Main and SE), common garden was the primary driver of spectral divergence in PC space.

Variance partitioning and broad-sense heritability

Across all gardens, spectral variance was highest in the visible (~500-670 nm) and red-edge wavelengths (~680-750 nm). When Yuma was included in the analysis, variance in these wavelengths was driven largely by the common garden site (Figures 2 and 3), and heritability in these regions was correspondingly low with a maximum heritability of 0.08 and 0.43 for the visible and red-edge, respectively (Figure 4). While heritability peaks near the red edge were present regardless of the inclusion of Yuma in the analysis, the peak was shifted toward shorter wavelengths when Yuma was excluded. Additionally, site-level variation in the visible (~500-670 nm) and red-edge wavelengths (~680-750 nm) was minimal without Yuma. Instead, variance at these wavelengths was driven more by genetic factors (population and genotype), with corresponding high spectral heritability (~0.36 and ~0.66, respectively).

Across all gardens, heritability in *P. fremontii* reflectance was greatest in the SWIR (1400 – 2450 nm), followed by the transition from red-edge to NIR (~750 nm), regardless of the inclusion of Yuma (Figure 4). In the shorter wavelengths of the NIR (~750-1140 nm) and SWIR, site-level variation explained less of the variance than genotypic factors in general, and the spectral differences caused by Yuma were relatively minimal, resulting in high heritability (max: 0.51; min: 0.31). When Yuma was excluded, heritability peaked in the red-edge (740 nm; heritability: 0.67). Heritability had a negative relationship with wavelength in the NIR until ~1320 nm where heritability increased and remained high in the SWIR, although it varied across this region (max: ~0.56, min: ~0.37). Across the VSWIR, particularly heritable regions of the

spectra included the red-edge/NIR transition (~750 nm) and the SWIR. More environmentally sensitive (plastic) regions included the visible and red-edge as well as much of the NIR.

SVM analysis and leaf predictions

SVM models were able to discriminate between spectra based on both common garden site and source population at 92.6% and 71.8% accuracy, respectively (Figure 4). The SVM trained to classify spectra based on the common garden site (environmental variation) outperformed the SVM trained to discriminate spectra based on source population (genotypic variation). The common garden site SVM accurately predicted spectra from the Yuma site 100% of the time; confusion in this model occurred primarily between Canyonlands and Agua Fria, with the true positive rate for Canyonlands and Agua Fria being 94% and 84%, respectively. For the source population SVM, the true positive rate ranged from 61% for the KWF population to 84% for CLF. When predicting source population using one common garden site as a holdout for testing, model performance declined. Source populations at Canyonlands were predicted with 36.0% accuracy when trained on data from Agua Fria and Yuma. At Agua Fria and Yuma, accuracy was 32.8% and 37.5%, respectively, when SVM models were trained on data from the other common garden sites.

Discussion

P. fremontii intraspecific variation in reflectance spectra was driven by the interaction between common garden site conditions and source population. The heritability of spectra varied across the VSWIR and depended on common garden site, with extreme temperatures, here defined as the point where the ambient temperatures are at the upper threshold of the *P. fremontii*

thermal tolerance (Moran et al., 2023), at Yuma likely causing a threshold change in spectral expression and heritability. Comparisons between the Agua Fria and Canyonlands sites revealed greater spectral separation based on ecotype than between the common gardens. However, within finer sub-ecotype categories, differences were primarily driven by the common garden, reinforcing the interconnected roles of genetics and environment in shaping spectral traits. We further demonstrated the strong environmental influence on spectral variation using SVM models. While the SVMs classified *P. fremontii* source population with 78% accuracy among all the common gardens, models built using spectra from two common gardens failed to generalize to the third (<37% accuracy). Lastly, we determined that *P. fremontii* spectra had low heritability in the visible and were most heritable in the SWIR. While heritability peaked in the red edge, the location of the peak was sensitive to extreme temperatures.

Heritability and plasticity of reflectance spectra

P. fremontii reflectance demonstrated both plastic (responsive to common garden site) and genotypic responses. The degree of plasticity exhibited by the spectra was influenced by the inclusion of reflectance data from Yuma. In the first PCA analysis, the first two PCs primarily separated the spectra according to whether the spectra were collected at Yuma or not, likely due to the extreme heat experienced by the trees at Yuma. Similarly, Li et al. (2023) examined genetic variation of *Nicotiana attenuata* (wilt tobacco) across common garden sites in Arizona and Utah, and they found that PC1 of the spectra was primarily influenced by the location of the common garden. *N. attenuata* genotype affected clustering of PC 2-4, indicating that environment had the primary effect on leaf reflectance while genotype had a secondary effect (Li et al., 2023). Extreme heat additionally caused an increase in visible and SWIR albedo across all

populations. Yuma is near the southern edge of the distribution of *P. fremontii* where it may not survive future climatic conditions (e.g., Blasini et al., 2021; Moran et al., 2023), so identifying environmental indicators of extreme environmental conditions may allow us to monitor stress at the shifting range edge of *P. fremontii.*

Below this physiological temperature threshold, spectral differences were predominantly governed by genetic factors, with environmental conditions playing a significant role in shaping phenotypic expression within genetically similar groups. Excluding Yuma in the PCA resulted in the source population (genotype) being the primary driver of separability, observed by the separation of the Sonoran Desert and Colorado Plateau ecotypes in PC space. For the finer-scale comparison of sub-ecotypes within the Sonoran Desert ecotypes, the environmental influence became dominant; the two Sonoran Desert ecotypes were separated first by common garden site (environment) and second by ecotype (genotype). This nested effect of genotype and environment on phenotypic variation can help us understand how ecotypes adapt to future climate scenarios, where genetic predispositions and environmental variability shape ecological outcomes.

Across the VSWIR, we observed greater sensitivity to temperature in the visible and red-edge regions as broad sense heritability across those wavelengths shifted in response to the inclusion of Yuma in the analysis. As the visible region of the spectra evolved largely to optimize light capture, this region has been strongly influenced by evolutionary forces (Meireles et al., 2020). As such, heritability in the visible region has been well-documented in other species (Čepl et al., 2018; Feng et al., 2017; McManus et al., 2016). For example, *Metrosideros polymorpha* varieties that organize along environmental gradients diverged in chlorophyll content, which was associated with differences in the visible wavelengths (Seeley et al. 2023b).

Here and in other studies, the visible region has also been highly sensitive to changing environmental conditions, likely due to mechanisms that help protect plants from heat stress (Mathur et al., 2014), suggesting that the visible range may not only be indicative of heat stress but also potential adaptability to future increases in temperature.

Similarly, the red edge can be both heritable (Čepl et al., 2018; Czyż et al., 2020; Feng et al., 2017) and indicative of stress (Abdullah et al., 2019; Dobrowski et al., 2005; Smith et al., 2004). For example, Feng et al. (2017) found that the red edge was predictive of rice genotypes, and both Čepal et al. (2018) and Czyż et al. (2020) observed a red edge signal in the heritability of *Pinus sylvestris* (Scotts pine) and *Fagus sylvatica* (European beech) leaf reflectance, respectively. We observed high heritability in the red edge relative to the rest of the VSWIR spectra, though this peak was narrower and shifted toward longer wavelengths when Yuma was included in the analysis, likely due to thermal stress. The shift in the red-edge heritability peak requires further investigation as it may challenge large-scale health monitoring where vegetation is genetically diverse and genotype classifications where stress varies.

P. fremontii heritability in the NIR also peaked at 1350 nm. These heritability peaks are similar to those of both *Pinus sylvestris* and *F. sylvatica* (Čepl et al., 2018; Czyż et al., 2020), though *Pinus sylvestris* had an additional region of high heritability around 1130-1330 in the NIR that corresponded to low heritability in *P. fremontii*. As much of the NIR corresponds to leaf structure (Knipling, 1970; Slaton et al., 2001), differences in heritability between *P. fremontii* and *Pinus sylvestris* may relate to differences between broad and needle leaves.

Overall, heritability in the SWIR was high relative to other wavelengths, especially when Yuma was included in the analysis. Spectral variation due to source population and genotype (genetic factors) was greater than variation stemming from common garden sites (environmental

factors) across the NIR and SWIR, regardless of the inclusion of Yuma. When predicting the genetic structure of *F. sylvatica* using the airborne prism experiment imaging spectrometer, longer wavelengths (> ~1900nm) in the SWIR were more predictive (Czyż et al., 2020). McManus et al. (2016) likewise found that the phylogenetic signal was greatest in the SWIR across many Neotropical tree species, and Meireles et al. (2020) observed a phylogenetic signal in Rosids, a clade of flowering plants that includes *Populus*, in the shorter wavelengths of the SWIR. The high heritability in the SWIR, consistent regardless of temperature stress, suggests that plant traits not directly related to photosynthesis (e.g. lignin, cellulose, and tannins; Asner and Martin, 2016, 2009) may be driving, in part, phylogenetic signals.

Overall, environmental conditions exerted a stronger control over *P. fremontii* intraspecific spectral variation. Much of the evidence presented above demonstrates the strong influence of the environment on spectral variation. Additionally, we found that SVM models based on common garden sites were ~14% more accurate than those separating source population spectra. Cavender-Bares et al. (2016) similarly found that while the source population of *Quercus oleoides* could be distinguished using PLS-DA models (kappa score = 0.342), watering treatment was predicted with greater accuracy (kappa score = 0.61). When the SVM was trained on data from two common garden sites and tested on the third, accuracy in predicting *P. fremontii* source population declined by over 34%, supporting other studies that have demonstrated how the environmental sensitivity of spectra limits large-scale species classifications (e.g. Seeley et al., 2024). While plastic responses to heat stress may decrease spectral heritability, environmentally sensitive regions of the spectra offer opportunities to understand physiological responses to extreme temperatures at large scales and may serve as environmental indicators of stress events.

Environmental thresholds

When exposed to extreme heat, plants employ a variety of mechanisms to increase their tolerance. Plastic responses at the individual level include increased LMA (observed at Yuma), increased heat shock proteins (HSP) to help repair heat damage, concentrations of which have been found to correlate with LMA (Knight & Ackerly, 2003), trichome development to promote self-shading (Banowetz et al., 2008), an accumulation of phenolics and isoprenoids for their ability to protect photosynthetic apparatuses and antioxidant properties (Bartwal et al., 2013; Smirnoff, 2005), and increased production of soluble sugars (Wahid & Close, 2007) and saturated fatty acids (Ahmad & Prasad, 2011; Tang et al., 2016). As many of the physical and chemical changes such as increased LMA, plant phenols, soluble sugars, and fatty acids can be estimated using spectroscopy (Akkaya, 2018; Asner & Martin, 2009, 2016), it is unsurprising that *P. fremontii* at Yuma differed spectrally from those at the other sites. For *Panax ginseng*, differences between VSWIR reflectance of heat-stressed and control plants corresponded to spectral regions linked to fatty acids, sugars, protein, chlorophyll, and nitrogen (Park et al., 2021). Similarly, other studies have found differences between control and heat-stressed plants using fluorescence (Faqeerzada et al., 2023) and visible-NIR (Kim et al., 2022) spectroscopy.

P. fremontii LMA increased along the common garden temperature gradient, contrasting with many studies reporting a negative relationship between LMA and temperature (e.g. Poorter et al., 2009). This increase in LMA may reflect a response to water stress, as higher LMA is a strategy to reduce water loss under drought conditions (Poorter et al., 2009). While all gardens were irrigated, high temperatures and drought often co-occur. Knight and Ackerly (2003) observed increased LMA, which correlated with increases in photosynthetic recovery rates, in

desert plants when thermally stressed, identifying high LMA as a convergent trait in species like *P. fremontii* that are adapted to elevated temperatures and low precipitation.

The shift in reflectance between Yuma trees and those at the cooler sites primarily occurred in the visible and red-edge wavelengths, indicating that photosystems were likely disrupted. Together, the visible and red edges are predictive of chlorophyll and other photosynthetic pigments (Horler et al., 1983; Vogelmann et al., 1993). Both as a mechanism of photosynthetic apparatus protection and as a side effect of the stress response, trees at Yuma had higher reflectance in the visible range, similar to that of heat-stressed rice (Xie et al., 2019) and maize (Tirado et al., 2021). As photosystem II is vulnerable to heat, photosynthesis is often the first mechanism influenced by temperature (Mathur et al., 2014). Shifts in the red edge have been linked to plant stressors such as heat and water stress (Dobrowski et al., 2005), bark beetles (Abdullah et al., 2019), and natural gas leakage (Smith et al., 2004), all of which induced changes in chlorophyll (Carter, 1993; Carter & Miller, 1994). PRI, a plant stress indicator (Thénot et al., 2002), as well as the stunted growth of trees at Yuma compared to that at the other sites, supports the conclusion that trees at Yuma were more stressed than those at the other sites.

In the SWIR, site-level responses in spectral variation remained regardless of the inclusion of Yuma. Park et al. (2021) noted the importance of the SWIR for separating heat-stressed and control plants using spectroscopy. Further, temperature-dependent leaf traits of other *Populus* species, *P. tremuloides* and *P. deltoides*, were predictable using wavelengths in visible and SWIR regions (Serbin et al., 2012). Both of these studies linked temperature-related responses in the SWIR with plant traits known to respond to heat stress (Park et al., 2021; Serbin et al., 2012). Here, site-level variation between Agua Fria and Canyonlands was primarily

observed in the SWIR and, to a lesser degree, the NIR, emphasizing the importance of using the full spectrum to distinguish between temperature treatments.

Across the entire VSWIR spectra, albedo increased in response to extreme temperature, likely lowering canopy temperatures and helping mitigate further heat stress. In the NIR – SWIR, albedo decreased from Canyonlands to Agua Fria, supporting the results from Doughty et al. (2018), where albedo declined across a temperature gradient in Peru. Regardless of which region of the VSWIR was analyzed, albedo at Yuma was higher than at the other common gardens. While additional evidence is required to confirm whether the increase in leaf albedo is a universal plant response to extremely high temperatures, this phenomenon aligns with plant ecophysiological principles, as many stress factors are known to decrease chlorophyll concentration (Carter & Knapp, 2001).

Conclusions

Reflectance spectra of *P. fremontii* contain valuable information about both the environmental conditions in which they grow and their genetic identities. Intraspecific spectral variation of *P. fremontii* was shaped by both common garden site and source population, with environmental conditions playing a dominant role under extreme stress, such as the high temperatures at the Yuma site. At the upper thermal threshold of *P. fremontii*, the spectral response was most pronounced in the visible and red-edge regions, corresponding to documented heat stress responses. In these regions, spectral heritability decreased when Yuma was considered in the analysis, suggesting that extreme environmental conditions may drive a threshold shift in spectral expression. However, genetic information was retained, and heritability was more consistent in parts of the NIR and SWIR.

These results underscore the potential for using VSWIR reflectance data to disentangle genetic and environmental contributions to plant phenotypes, providing a path forward for scaling these insights to larger landscapes. As airborne and satellite-based imaging spectroscopy data continue to become more widely available, they offer a powerful opportunity to assess phenotypic plasticity and heritable resilience of *P. fremontii* to extreme conditions across broad spatial scales. Spectroscopy may be a powerful tool for monitoring the adaptive capacity of this foundation species in the face of rapid environmental change, supporting efforts to preserve and manage at-risk ecosystems in a warming climate.

Declarations

Funding: The common gardens were initially developed under NSF Macrosystems grant DEB 2017877 awarded to GJA, TGW, and KCG. Funding for this research was provided by the NSF MacroSystems grant DEB-1340852 awarded to GJA, TGW, and CED as well as the NSF DEB□1340856 awarded to KRH.

Author contributions: Original idea: CED, ET, GPA; common garden development common gardens: GJA, TGW, KCG, KRH, and HFC; data collection: ET; statistical analysis: MMS, ET, methodology: MMS, ET, CED, BCW; writing the manuscript: MMS, ET. All authors reviewed several drafts and agreed with the final version.

Availability of data: All data files will be made available on the Figshare database upon acceptance of the manuscript at DOI: 10.6084/m9.figshare.25719585.

Code availability: Code is available on GitHub and is maintained by Seeley (2025) https://github.com/MegsSeeley/temperature_cottonwood.

Conflict of interest: The authors have declared that no competing interests exist.

References

Abdullah, H., Skidmore, A. K., Darvishzadeh, R., & Heurich, M. (2019). Timing of red-edge and shortwave infrared reflectance critical for early stress detection induced by bark beetle (Ips typographus, L.) attack. *International Journal of Applied Earth Observation and Geoinformation*, *82*, 101900. https://doi.org/10.1016/j.jag.2019.101900

Ahmad, P., & Prasad, M. N. V. (2011). *Environmental Adaptations and Stress Tolerance of Plants in the Era of Climate Change*. Springer Science & Business Media.

Akkaya, M. R. (2018). Prediction of fatty acid composition of sunflower seeds by near-infrared reflectance spectroscopy. *Journal of Food Science and Technology*, *55*(6), 2318–2325. https://doi.org/10.1007/s13197-018-3150-x

Allen, C. D., Macalady, A. K., Chenchouni, H., Bachelet, D., McDowell, N., Vennetier, M., … Cobb, N. (2010). A global overview of drought and heat-induced tree mortality reveals emerging climate change risks for forests. *Forest Ecology and Management*, *259*(4), 660–684. https://doi.org/10.1016/j.foreco.2009.09.001

Asner, G. P., & Martin, R. E. (2009). Airborne spectranomics: Mapping canopy chemical and taxonomic diversity in tropical forests. *Frontiers in Ecology and the Environment*, *7*(5), 269–276. https://doi.org/10.1890/070152

Asner, G. P., & Martin, R. E. (2016). Spectranomics: Emerging science and conservation opportunities at the interface of biodiversity and remote sensing. *Global Ecology and Conservation*, *8*, 212–219. https://doi.org/10.1016/j.gecco.2016.09.010

Asner, G. P., Martin, R. E., Tupayachi, R., Anderson, C. B., Sinca, F., Carranza-Jiménez, L., & Martinez, P. (2014). Amazonian functional diversity from forest canopy chemical

assembly. *Proceedings of the National Academy of Sciences*, *111*(15), 5604–5609. https://doi.org/10.1073/pnas.1401181111

Asner, G. P., Martin, R. E., Tupayachi, R., & Llactayo, W. (2017). Conservation assessment of the Peruvian Andes and Amazon based on mapped forest functional diversity. *Biological Conservation*, *210*, 80–88. https://doi.org/10.1016/j.biocon.2017.04.008

Balzotti, C. S., Asner, G. P., Adkins, E. D., & Parsons, E. W. (2020). Spatial drivers of composition and connectivity across endangered tropical dry forests. *Journal of Applied Ecology*, *57*(8), 1593–1604. https://doi.org/10.1111/1365-2664.13632

Banowetz, G. M., Azevedo, M. D., & Stout, R. (2008). Morphological adaptations of hot springs panic grass (Dichanthelium lanigunosum var sericeum (Schmoll) to thermal stress. *Journal of Thermal Biology*, *33*(2), 106–116. https://doi.org/10.1016/j.jtherbio.2007.08.006

Bartlett, M. K., Ollinger, S. V., Hollinger, D. Y., Wicklein, H. F., & Richardson, A. D. (2011). Canopy-scale relationships between foliar nitrogen and albedo are not observed in leaf reflectance and transmittance within temperate deciduous tree species. *Botany*, *89*(7), 491–497. https://doi.org/10.1139/b11-037

Bartwal, A., Mall, R., Lohani, P., Guru, S. K., & Arora, S. (2013). Role of Secondary Metabolites and Brassinosteroids in Plant Defense Against Environmental Stresses. *Journal of Plant Growth Regulation*, *32*(1), 216–232. https://doi.org/10.1007/s00344-012-9272-x

Bates, D., Mächler, M., Bolker, B., & Walker, S. (2015). Fitting Linear Mixed-Effects Models Using lme4. *Journal of Statistical Software*, *67*, 1–48. https://doi.org/10.18637/jss.v067.i01

Blasini, D. E., Koepke, D. F., Grady, K. C., Allan, G. J., Gehring, C. A., Whitham, T. G., … Hultine, K. R. (2021). Adaptive trait syndromes along multiple economic spectra define cold and warm adapted ecotypes in a widely distributed foundation tree species. *Journal of Ecology*, *109*(3), 1298–1318. https://doi.org/10.1111/1365-2745.13557

Blonder, B., Graae, B. J., Greer, B., Haagsma, M., Helsen, K., Kapás, R. E., … Strimbeck, R. (2020). Remote sensing of ploidy level in quaking aspen (Populus tremuloides Michx.). *Journal of Ecology*, *108*(1), 175–188. https://doi.org/10.1111/1365-2745.13296

Boardman, J. W., & Green, R. O. (2000). *Exploring the spectral variability of the Earth as measured by AVIRIS in 1999*. https://trs.jpl.nasa.gov/handle/2014/16602

Bothwell, H. M., Keith, A. R., Cooper, H. F., Hull, J. B., Andrews, L. V., Wehenkel, C., … Allan, G. J. (2023). Microevolutionary Processes in a Foundation Tree Inform Macrosystem Patterns of Community Biodiversity and Structure. *Forests*, *14*(5), Article 5. https://doi.org/10.3390/f14050943

Braatne, J., Rood, S., & Heilman, P. (1996). *Life history, ecology, and conservation of riparian cottonwoods in North America* (pp. 57–85).

Bradshaw, J. E. (2017). Plant breeding: Past, present and future. *Euphytica*, *213*(3), 60. https://doi.org/10.1007/s10681-016-1815-y

Brodrick, P. G., & Asner, G. P. (2017). Remotely sensed predictors of conifer tree mortality during severe drought. *Environmental Research Letters*, *12*(11), 115013. https://doi.org/10.1088/1748-9326/aa8f55

Buddenbaum, H., Rock, G., Hill, J., & Werner, W. (2015). Measuring Stress Reactions of Beech Seedlings with PRI, Fluorescence, Temperatures and Emissivity from VNIR and Thermal

Field Imaging Spectroscopy. *European Journal of Remote Sensing*, *48*(1), 263–282. https://doi.org/10.5721/EuJRS20154815

Carter, G. A. (1993). Responses of Leaf Spectral Reflectance to Plant Stress. *American Journal of Botany*, *80*(3), 239–243. https://doi.org/10.1002/j.1537-2197.1993.tb13796.x

Carter, G. A., & Knapp, A. K. (2001). Leaf optical properties in higher plants: Linking spectral characteristics to stress and chlorophyll concentration. *American Journal of Botany*, *88*(4), 677–684. https://doi.org/10.2307/2657068

Carter, G. A., & Miller, R. L. (1994). Early detection of plant stress by digital imaging within narrow stress-sensitive wavebands. *Remote Sensing of Environment*, *50*(3), 295–302. https://doi.org/10.1016/0034-4257(94)90079-5

Cavender-Bares, J., Meireles, J. E., Couture, J. J., Kaproth, M. A., Kingdon, C. C., Singh, A., … Townsend, P. A. (2016). Associations of Leaf Spectra with Genetic and Phylogenetic Variation in Oaks: Prospects for Remote Detection of Biodiversity. *Remote Sensing*, *8*(3), Article 3. https://doi.org/10.3390/rs8030221

Čepl, J., Stejskal, J., Lhotáková, Z., Holá, D., Korecký, J., Lstibůrek, M., … Albrechtová, J. (2018). Heritable variation in needle spectral reflectance of Scots pine (Pinus sylvestris L.) peaks in red edge. *Remote Sensing of Environment*, *219*, 89–98. https://doi.org/10.1016/j.rse.2018.10.001

Cooper, H. F., Best, R. J., Andrews, L. V., Corbin, J. P. M., Garthwaite, I., Grady, K. C., … Allan, G. J. (2022). Evidence of climate-driven selection on tree traits and trait plasticity across the climatic range of a riparian foundation species. *Molecular Ecology*, *31*(19), 5024–5040. https://doi.org/10.1111/mec.16645

Cooper, H. F., Grady, K. C., Cowan, J. A., Best, R. J., Allan, G. J., & Whitham, T. G. (2019). Genotypic variation in phenological plasticity: Reciprocal common gardens reveal adaptive responses to warmer springs but not to fall frost. *Global Change Biology*, *25*(1), 187–200. https://doi.org/10.1111/gcb.14494

Czyż, E. A., Guillén Escribà, C., Wulf, H., Tedder, A., Schuman, M. C., Schneider, F. D., & Schaepman, M. E. (2020). Intraspecific genetic variation of a Fagus sylvatica population in a temperate forest derived from airborne imaging spectroscopy time series. *Ecology and Evolution*, *10*(14), 7419–7430. https://doi.org/10.1002/ece3.6469

Dai, J., Vaughn, N. R., Seeley, M., Heckler, J., Thompson, D. R., & Asner, G. P. (2022). Spectral dimensionality of imaging spectroscopy data over diverse landscapes and spatial resolutions. *Journal of Applied Remote Sensing*, *16*(4), 044518. https://doi.org/10.1117/1.JRS.16.044518

Dalponte, M., Bruzzone, L., & Gianelle, D. (2012). Tree species classification in the Southern Alps based on the fusion of very high geometrical resolution multispectral/hyperspectral images and LiDAR data. *Remote Sensing of Environment*, *123*, 258–270. https://doi.org/10.1016/j.rse.2012.03.013

Dobrowski, S. Z., Pushnik, J. C., Zarco-Tejada, P. J., & Ustin, S. L. (2005). Simple reflectance indices track heat and water stress-induced changes in steady-state chlorophyll fluorescence at the canopy scale. *Remote Sensing of Environment*, *97*(3), 403–414. https://doi.org/10.1016/j.rse.2005.05.006

Doughty, C. E., Santos-Andrade, P. E., Shenkin, A., Goldsmith, G. R., Bentley, L. P., Blonder, B., … Malhi, Y. (2018). Tropical forest leaves may darken in response to climate change.

Nature Ecology & Evolution, *2*(12), 1918–1924. https://doi.org/10.1038/s41559-018-0716-y

Ellison, A. M., Bank, M. S., Clinton, B. D., Colburn, E. A., Elliott, K., Ford, C. R., … Webster, J. R. (2005). Loss of foundation species: Consequences for the structure and dynamics of forested ecosystems. *Frontiers in Ecology and the Environment*, *3*(9), 479–486. https://doi.org/10.1890/1540-9295(2005)003[0479:LOFSCF]2.0.CO;2

Faqeerzada, M. A., Park, E., Kim, T., Kim, M. S., Baek, I., Joshi, R., … Cho, B.-K. (2023). Fluorescence Hyperspectral Imaging for Early Diagnosis of Heat-Stressed Ginseng Plants. *Applied Sciences*, *13*(1), Article 1. https://doi.org/10.3390/app13010031

Feng, H., Guo, Z., Yang, W., Huang, C., Chen, G., Fang, W., … Liu, Q. (2017). An integrated hyperspectral imaging and genome-wide association analysis platform provides spectral and genetic insights into the natural variation in rice. *Scientific Reports*, *7*(1), Article 1. https://doi.org/10.1038/s41598-017-04668-8

Féret, J.-B., & Asner, G. P. (2014). Mapping tropical forest canopy diversity using high-fidelity imaging spectroscopy. *Ecological Applications*, *24*(6), 1289–1296. https://doi.org/10.1890/13-1824.1

Ferrier, S. M., Bangert, R. K., Hersch-Green, E. I., Bailey, J. K., Allan, G. J., & Whitham, T. G. (2012). Unique arthropod communities on different host-plant genotypes results in greater arthropod diversity. *Arthropod-Plant Interactions*, *6*(2), 187–195. https://doi.org/10.1007/s11829-011-9177-9

Fyllas, N. M., Patiño, S., Baker, T. R., Bielefeld Nardoto, G., Martinelli, L. A., Quesada, C. A., … Lloyd, J. (2009). Basin-wide variations in foliar properties of Amazonian forest:

Phylogeny, soils and climate. *Biogeosciences*, *6*, 2677–2708. https://doi.org/10.5194/bg-6-2677-200910.5194/bgd-6-3707-2009

Gamon, J. A., Peñuelas, J., & Field, C. B. (1992). A narrow-waveband spectral index that tracks diurnal changes in photosynthetic efficiency. *Remote Sensing of Environment*, *41*(1), 35–44. https://doi.org/10.1016/0034-4257(92)90059-S

Grady, K. C., Laughlin, D. C., Ferrier, S. M., Kolb, T. E., Hart, S. C., Allan, G. J., & Whitham, T. G. (2013). Conservative leaf economic traits correlate with fast growth of genotypes of a foundation riparian species near the thermal maximum extent of its geographic range. *Functional Ecology*, *27*(2), 428–438. https://doi.org/10.1111/1365-2435.12060

Green, R. O., & Boardman, J. W. (2000). Exploration of the relationship between information content and signal-to-noise ratio and spatial resolution in AVIRIS spectral data. *Spectrum*, *7*(8).

Gueymard, C. A. (2004). The sun's total and spectral irradiance for solar energy applications and solar radiation models. *Solar Energy*, *76*(4), 423–453. https://doi.org/10.1016/j.solener.2003.08.039

Hernández-Clemente, R., Navarro-Cerrillo, R. M., Suárez, L., Morales, F., & Zarco-Tejada, P. J. (2011). Assessing structural effects on PRI for stress detection in conifer forests. *Remote Sensing of Environment*, *115*(9), 2360–2375. https://doi.org/10.1016/j.rse.2011.04.036

Horler, D. N. H., Dockray, M., & Barber, J. (1983). The red edge of plant leaf reflectance. *International Journal of Remote Sensing*, *4*(2), 273–288. https://doi.org/10.1080/01431168308948546

Hühn, M. (1975). Estimation of broad sense heritability in plant populations: An improved method. *Theoretical and Applied Genetics*, *46*(2), 87–99. https://doi.org/10.1007/BF00281647

Hultine, K. R., Allan, G. J., Blasini, D., Bothwell, H. M., Cadmus, A., Cooper, H. F., … Whitham, T. G. (2020). Adaptive capacity in the foundation tree species Populus fremontii: Implications for resilience to climate change and non-native species invasion in the American Southwest. *Conservation Physiology*, *8*(1), coaa061. https://doi.org/10.1093/conphys/coaa061

Ikeda, D. H., Max, T. L., Allan, G. J., Lau, M. K., Shuster, S. M., & Whitham, T. G. (2017). Genetically informed ecological niche models improve climate change predictions. *Global Change Biology*, *23*(1), 164–176. https://doi.org/10.1111/gcb.13470

Kim, G., Lee, H., Wi, S. H., & Cho, B.-K. (2022). Snapshot-Based Visible-Near Infrared Multispectral Imaging for Early Screening of Heat Injury during Growth of Chinese Cabbage. *Applied Sciences*, *12*(18), Article 18. https://doi.org/10.3390/app12189340

Knight, C. A., & Ackerly, D. D. (2003). Evolution and plasticity of photosynthetic thermal tolerance, specific leaf area and leaf size: Congeneric species from desert and coastal environments. *New Phytologist*, *160*(2), 337–347. https://doi.org/10.1046/j.1469-8137.2003.00880.x

Knipling, E. B. (1970). Physical and physiological basis for the reflectance of visible and near-infrared radiation from vegetation. *Remote Sensing of Environment*, *1*(3), 155–159. https://doi.org/10.1016/S0034-4257(70)80021-9

Kruse, F. A., Heidebrecht, K. B., Shapiro, A. T., Barloon, P. J., & Goetz, A. F. H. (1993). The Spectral Image Processing System (SIPS) Interactive Visualization and Analysis of Imaging Spectrometer Data. *Remote Sensing of Environment*, *44*, 145–163.

Li, C., Czyż, E. A., Halitschke, R., Baldwin, I. T., Schaepman, M. E., & Schuman, M. C. (2023). Evaluating potential of leaf reflectance spectra to monitor plant genetic variation. *Plant Methods*, *19*(1), 108. https://doi.org/10.1186/s13007-023-01089-9

Mathur, S., Agrawal, D., & Jajoo, A. (2014). Photosynthesis: Response to high temperature stress. *Journal of Photochemistry and Photobiology B: Biology*, *137*, 116–126. https://doi.org/10.1016/j.jphotobiol.2014.01.010

McManus, K. M., Asner, G. P., Martin, R. E., Dexter, K. G., Kress, W. J., & Field, C. B. (2016). Phylogenetic Structure of Foliar Spectral Traits in Tropical Forest Canopies. *Remote Sensing*, *8*(3), Article 3. https://doi.org/10.3390/rs8030196

Meireles, J. E., Cavender-Bares, J., Townsend, P. A., Ustin, S., Gamon, J. A., Schweiger, A. K., … O'Meara, B. C. (2020). Leaf reflectance spectra capture the evolutionary history of seed plants. *New Phytologist*, *228*(2), 485–493. https://doi.org/10.1111/nph.16771

Melgani, F., & Bruzzone, L. (2004). Classification of hyperspectral remote sensing images with support vector machines. *IEEE Transactions on Geoscience and Remote Sensing*, *42*(8), 1778–1790. IEEE Transactions on Geoscience and Remote Sensing. https://doi.org/10.1109/TGRS.2004.831865

Moran, M. E., Aparecido, L. M. T., Koepke, D. F., Cooper, H. F., Doughty, C. E., Gehring, C. A., … Hultine, K. R. (2023). Limits of thermal and hydrological tolerance in a foundation tree species (Populus fremontii) in the desert southwestern United States. *New Phytologist*, *240*(6), 2298–2311. https://doi.org/10.1111/nph.19247

Myneni, R. B., Ross, J., & Asrar, G. (1989). A review on the theory of photon transport in leaf canopies. *Agricultural and Forest Meteorology*, *45*(1–2), 1–153. https://doi.org/10.1016/0168-1923(89)90002-6

Park, E., Kim, Y.-S., Omari, M. K., Suh, H.-K., Faqeerzada, M. A., Kim, M. S., … Cho, B.-K. (2021). High-Throughput Phenotyping Approach for the Evaluation of Heat Stress in Korean Ginseng (Panax ginseng Meyer) Using a Hyperspectral Reflectance Image. *Sensors*, *21*(16), Article 16. https://doi.org/10.3390/s21165634

Pedregosa, F., Varoquaux, G., Gramfort, A., Michel, V., Thirion, B., Grisel, O., … Duchesnay, É. (2011). Scikit-learn: Machine Learning in Python. *Journal of Machine Learning Research*, *12*(85), 2825–2830.

Pimm, S. L., Jenkins, C. N., Abell, R., Brooks, T. M., Gittleman, J. L., Joppa, L. N., … Sexton, J. O. (2014). The biodiversity of species and their rates of extinction, distribution, and protection. *Science*, *344*(6187), 1246752. https://doi.org/10.1126/science.1246752

Poorter, H., Niinemets, Ü., Poorter, L., Wright, I. J., & Villar, R. (2009). Causes and consequences of variation in leaf mass per area (LMA): A meta-analysis. *New Phytologist*, *182*(3), 565–588. https://doi.org/10.1111/j.1469-8137.2009.02830.x

Roberts, D. A., Dennison, P. E., Gardner, M. E., Hetzel, Y., Ustin, S. L., & Lee, C. T. (2003). Evaluation of the potential of Hyperion for fire danger assessment by comparison to the Airborne Visible/Infrared Imaging Spectrometer. *IEEE Transactions on Geoscience and Remote Sensing*, *41*(6), 1297–1310. IEEE Transactions on Geoscience and Remote Sensing. https://doi.org/10.1109/TGRS.2003.812904

Rose, R. A., Byler, D., Eastman, J. R., Fleishman, E., Geller, G., Goetz, S., … Wilson, C. (2015). Ten ways remote sensing can contribute to conservation. *Conservation Biology*, *29*(2), 350–359. https://doi.org/10.1111/cobi.12397

Rossini, M., Fava, F., Cogliati, S., Meroni, M., Marchesi, A., Panigada, … Colombo, R. (2013). Assessing canopy PRI from airborne imagery to map water stress in maize. *ISPRS Journal of Photogrammetry and Remote Sensing*, *86*, 168–177. https://doi.org/10.1016/j.isprsjprs.2013.10.002

Schweiger, R., Kaufman, S., Laaksonen, R., Kleber, M. E., März, W., Eskin, E., … Halperin, E. (2016). Fast and Accurate Construction of Confidence Intervals for Heritability. *American Journal of Human Genetics*, *98*(6), 1181–1192. https://doi.org/10.1016/j.ajhg.2016.04.016

Seeley, M., & Asner, G. P. (2021). Imaging Spectroscopy for Conservation Applications. *Remote Sensing*, *13*(2), Article 2. https://doi.org/10.3390/rs13020292

Seeley, M. M., & Asner, G. P. (2023). Large-Scale Controls on the Leaf Economic Spectrum of the Overstory Tree Species Metrosideros polymorpha. *Remote Sensing*, *15*(19), Article 19. https://doi.org/10.3390/rs15194707

Seeley, M. M., Martin, R. E., Vaughn, N. R., Thompson, D. R., Dai, J., & Asner, G. P. (2023a). Quantifying the Variation in Reflectance Spectra of Metrosideros polymorpha Canopies across Environmental Gradients. *Remote Sensing*, *15*(6), Article 6. https://doi.org/10.3390/rs15061614

Seeley, M. M., Stacy, E. A., Martin, R. E., & Asner, G. P. (2023b). Foliar functional and genetic variation in a keystone Hawaiian tree species estimated through spectroscopy. *Oecologia*. https://doi.org/10.1007/s00442-023-05374-1

Seeley, M. M., Vaughn, N. R., & Asner, G. A. (2024). Evaluating individual tree species classification performance across diverse environments. *Environmental Research: Ecology*, *3*(1), 011001. https://doi.org/10.1088/2752-664X/ad1f49

Seeley, M. M., Vaughn, N. R., Shanks, B. L., Martin, R. E., König, M., & Asner, G. P. (2023c). Classifying a highly polymorphic tree species across landscapes using airborne imaging spectroscopy. *Remote Sensing*, *15*(8), 4365. https://doi.org/10.3390/rs15184365

Serbin, S. P., Dillaway, D. N., Kruger, E. L., & Townsend, P. A. (2012). Leaf optical properties reflect variation in photosynthetic metabolism and its sensitivity to temperature. *Journal of Experimental Botany*, *63*(1), 489–502. https://doi.org/10.1093/jxb/err294

Shafroth, P. B., Friedman, J. M., & Ischinger, L. S. (1995). Effects of Salinity on Establishment of Populus Fremontii (cottonwood) and Tamarix Ramosissima (saltcedar) in Southwestern United States. *The Great Basin Naturalist*, *55*(1), 58–65.

Slaton, M. R., Raymond Hunt Jr., E., & Smith, W. K. (2001). Estimating near-infrared leaf reflectance from leaf structural characteristics. *American Journal of Botany*, *88*(2), 278–284. https://doi.org/10.2307/2657019

Smirnoff, N. (2005). *Antioxidants and Reactive Oxygen Species in Plants*. John Wiley & Sons, Ltd. https://doi.org/10.1002/9780470988565.fmatter

Smith, K. L., Steven, M. D., & Colls, J. J. (2004). Use of hyperspectral derivative ratios in the red-edge region to identify plant stress responses to gas leaks. *Remote Sensing of Environment*, *92*(2), 207–217. https://doi.org/10.1016/j.rse.2004.06.002

Stromberg, J. (1998). Dynamics of Fremont cottonwood (*Populus fremontii*) and saltcedar (*Tamarix chinensis*) populations along the San Pedro River, Arizona. *Journal of Arid Environments*, *40*(2), 133–155. https://doi.org/10.1006/jare.1998.0438

Tang, T., Liu, P., Zheng, G., & Li, W. (2016). Two phases of response to long-term moderate heat: Variation in thermotolerance between Arabidopsis thaliana and its relative Arabis paniculata. *Phytochemistry*, *122*, 81–90. https://doi.org/10.1016/j.phytochem.2016.01.003

Thénot, F., Méthy, M., & Winkel, T. (2002). The Photochemical Reflectance Index (PRI) as a water-stress index. *International Journal of Remote Sensing - INT J REMOTE SENS*, *23*, 5135–5139. https://doi.org/10.1080/01431160210163100

Thompson, D. R., Boardman, J. W., Eastwood, M. L., & Green, R. O. (2017). A large airborne survey of Earth's visible-infrared spectral dimensionality. *Optics Express*, *25*(8), 9186. https://doi.org/10.1364/OE.25.009186

Tirado, S. B., Dennis, S. St., Enders, T. A., & Springer, N. M. (2021). Utilizing spatial variability from hyperspectral imaging to assess variation in maize seedlings. *The Plant Phenome Journal*, *4*(1), e20013. https://doi.org/10.1002/ppj2.20013

Turner, M. (2023). Heritable trait variation for climate resilience. *Nature Ecology & Evolution*, *7*(4), 492–492. https://doi.org/10.1038/s41559-023-02004-0

Turner, W., Spector, S., Gardiner, N., Fladeland, M., Sterling, E., & Steininger, M. (2003). Remote sensing for biodiversity science and conservation. *Trends in Ecology & Evolution*, *18*(6), 306–314. https://doi.org/10.1016/S0169-5347(03)00070-3

Vahsen, M. L., Blum, M. J., Megonigal, J. P., Emrich, S. J., Holmquist, J. R., Stiller, B., … McLachlan, J. S. (2023). Rapid plant trait evolution can alter coastal wetland resilience to sea level rise. *Science*, *379*(6630), 393–398. https://doi.org/10.1126/science.abq0595

Virtanen, P., Gommers, R., Oliphant, T. E., Haberland, M., Reddy, T., Cournapeau, D., … Vázquez-Baeza, Y. (2020). SciPy 1.0: Fundamental algorithms for scientific computing in Python. *Nature Methods*, *17*(3), 261–272. https://doi.org/10.1038/s41592-019-0686-2

Vogelmann, J. E., Rock, B. N., & Moss, D. M. (1993). Red edge spectral measurements from sugar maple leaves. *Remote Sensing*, *14*(8), 1563–1575. https://doi.org/10.1080/01431169308953986

Wahid, A., & Close, T. J. (2007). Expression of dehydrins under heat stress and their relationship with water relations of sugarcane leaves. *Biologia Plantarum*, *51*(1), 104–109. https://doi.org/10.1007/s10535-007-0021-0

Wang, Z., Townsend, P. A., & Kruger, E. L. (2022). Leaf spectroscopy reveals divergent inter- and intra-species foliar trait covariation and trait–environment relationships across NEON domains. *New Phytologist*, *235*(3), 923–938. https://doi.org/10.1111/nph.18204

Weingarten, E., Martin, R., Hughes, F., Vaughn, N., Schafron, E., & Asner, G. P. (2021). Early Detection of a Tree Pathogen using Airborne Remote Sensing. *Ecological Applications.*, *21*(2).

Whitham, T. G., Bailey, J. K., Schweitzer, J. A., Shuster, S. M., Bangert, R. K., LeRoy, C. J., … Wooley, S. C. (2006). A framework for community and ecosystem genetics: From genes to ecosystems. *Nature Reviews Genetics*, *7*(7), Article 7. https://doi.org/10.1038/nrg1877

Xie, X. j., Zhang, Y. h., Li, R. y., Shen, S. h., & Bao, Y. x. (2019). Prediction model of rice crude protein content, amylose content and actual yield under high temperature stress based on hyper-spectral remote sensing. *Quality Assurance and Safety of Crops & Foods*, *11*(6), 517–527. https://doi.org/10.3920/QAS2018.1295

Yan, Z., Guo, Z., Serbin, S. P., Song, G., Zhao, Y., Chen, Y., … Wu, J. (2021). Spectroscopy outperforms leaf trait relationships for predicting photosynthetic capacity across different forest types. *New Phytologist*, *232*(1), 134–147. https://doi.org/10.1111/nph.17579

Tables

Source Population	Elevation	Mean Annual Temperature (°C)	Mean Annual Precipitation (mm)	Ecotype
MRN	1774	10.4	593	Sonoran Desert Main
KKH	1920	10.7	258	Colorado Plateau
JLA	1507	12.3	212	Colorado Plateau
CLF	1299	14.1	176	Colorado Plateau
KWF	1126	15	243	Sonoran Desert KWF
BCE	1109	15.6	432	Sonoran Desert Main
PSA	1234	15.7	471	Sonoran Desert SE
TSZ	1219	16.9	322	Sonoran Desert SE
CAF	988	17.2	440	Sonoran Desert Main
TSE	986	17.5	402	Sonoran Desert SE
WHY	575	19.6	284	Sonoran Desert Main
CCU	696	19.9	349	Sonoran Desert Main
NRV	666	19.9	337	Sonoran Desert Main
SCT	26	22.1	88	Sonoran Desert Main
LBW	143	22.3	137	Sonoran Desert Main
CCR	70	22.6	97	Sonoran Desert Main
Common Garden Site				
Canyonlands	1581	10.7	225	
Agua Fria	998	17.2	453	
Yuma	49	22.8	93	

Table 1: Source population and study site environmental conditions. For source populations, the ecotype is listed.

Figure Captions

Figure 1: Source population and common garden site locations in Arizona and southern Utah. Background colors represent Köppen climate types.

Figure 2: a) Mean brightness normalized reflectance of each source population, colored by common garden site. See Figure S1 for reflectance prior to brightness normalization. Boxplots of albedo calculated across the b) visible and c) near-infrared-shortwave infrared, d) photosynthetic reflectance index (PRI), and e) leaf mass per area (LMA). Within each garden, boxplots are ordered according to source population mean annual temperature, with cooler populations on the left and warmer populations on the right. Gaps correspond to populations that were not sampled at a given garden. Boxplots represent a different number of sampled trees per population per site.

Figure 3: a) First and second principal components (PC) of leaf spectra colored according to the common garden site. b) Distance between the centroids of source population grouped by ecotype x common garden in PC space. Colors represent common garden (blue: Canyonlands, grey: Agua Fria). Shapes correspond to the ecotype (x: Colorado Plateau, circle: Sonoran Desert, triangle: Sonoran Desert SE).

Figure 4: Heritability of reflectance spectra (solid line) and its 95% bootstrapped confidence interval (grey fill), mean brightness normalized reflectance spectra (dotted line), and the source of variability (filled colors) from the visible to shortwave infrared for *P. fremontii* at a) all sites and b) Canyonlands and Agua Fria.

Figure 5: Support vector machine confusion matrix results for predicting a) common garden site and b) source population. Source populations are ordered left to right and top to bottom from lowest to highest mean annual temperature.

Figures

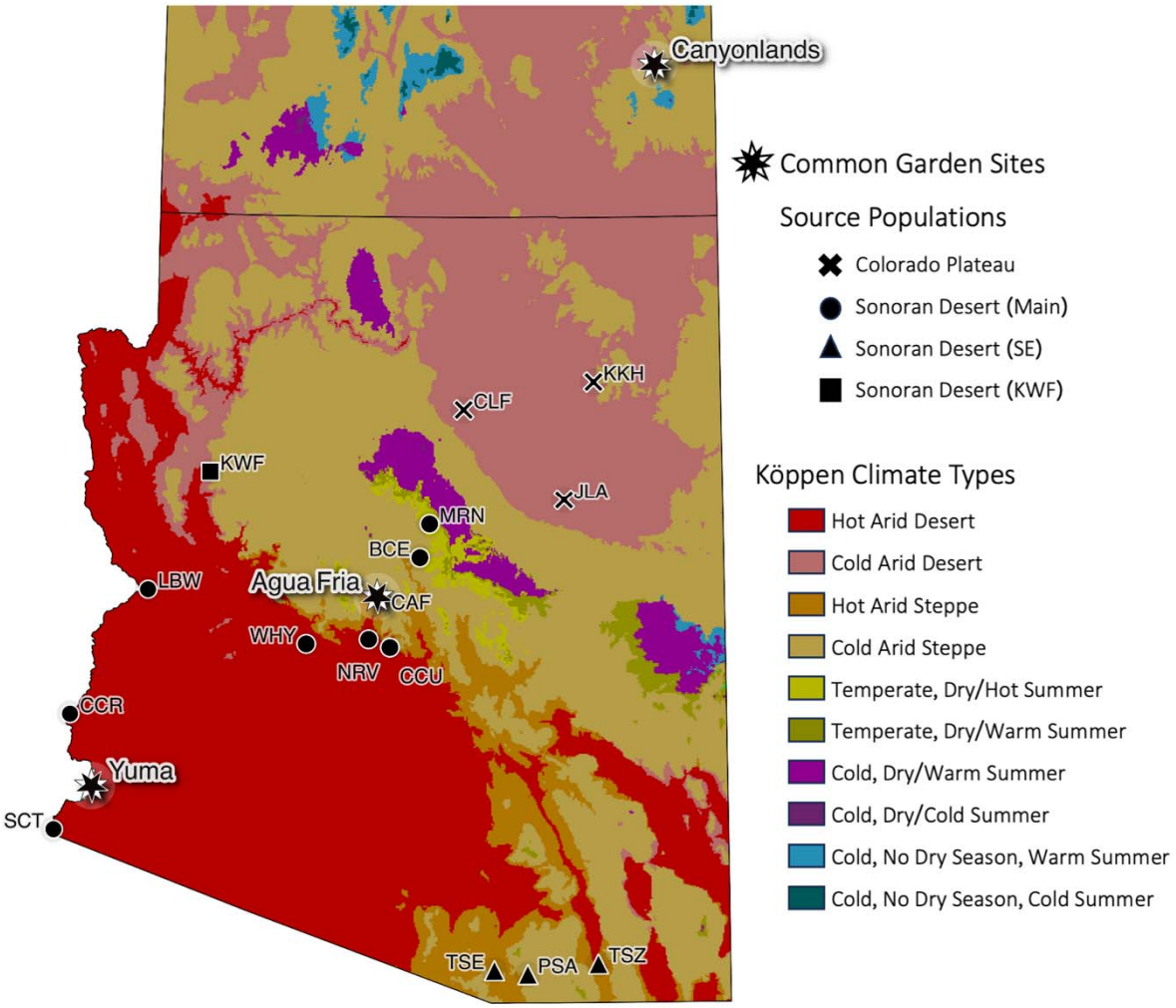
Canyonlands
Common Garden Sites
Source Populations
Colorado Plateau
Sonoran Desert (Main)
Sonoran Desert (SE)
Sonoran Desert (KWF)
Köppen Climate Types
Hot Arid Desert
Cold Arid Desert
Hot Arid Steppe
Cold Arid Steppe
Temperate, Dry/Hot Summer
Temperate, Dry/Warm Summer
Cold, Dry/Warm Summer
Cold, Dry/Cold Summer
Cold, No Dry Season, Warm Summer
Cold, No Dry Season, Cold Summer
KKH
CLF
KWF
JLA
MRN
BCE
LBW
Agua Fria
CAF
WHY
NRV
CCU
CCR
Yuma
SCT
TSE
PSA
TSZ

Figure 1

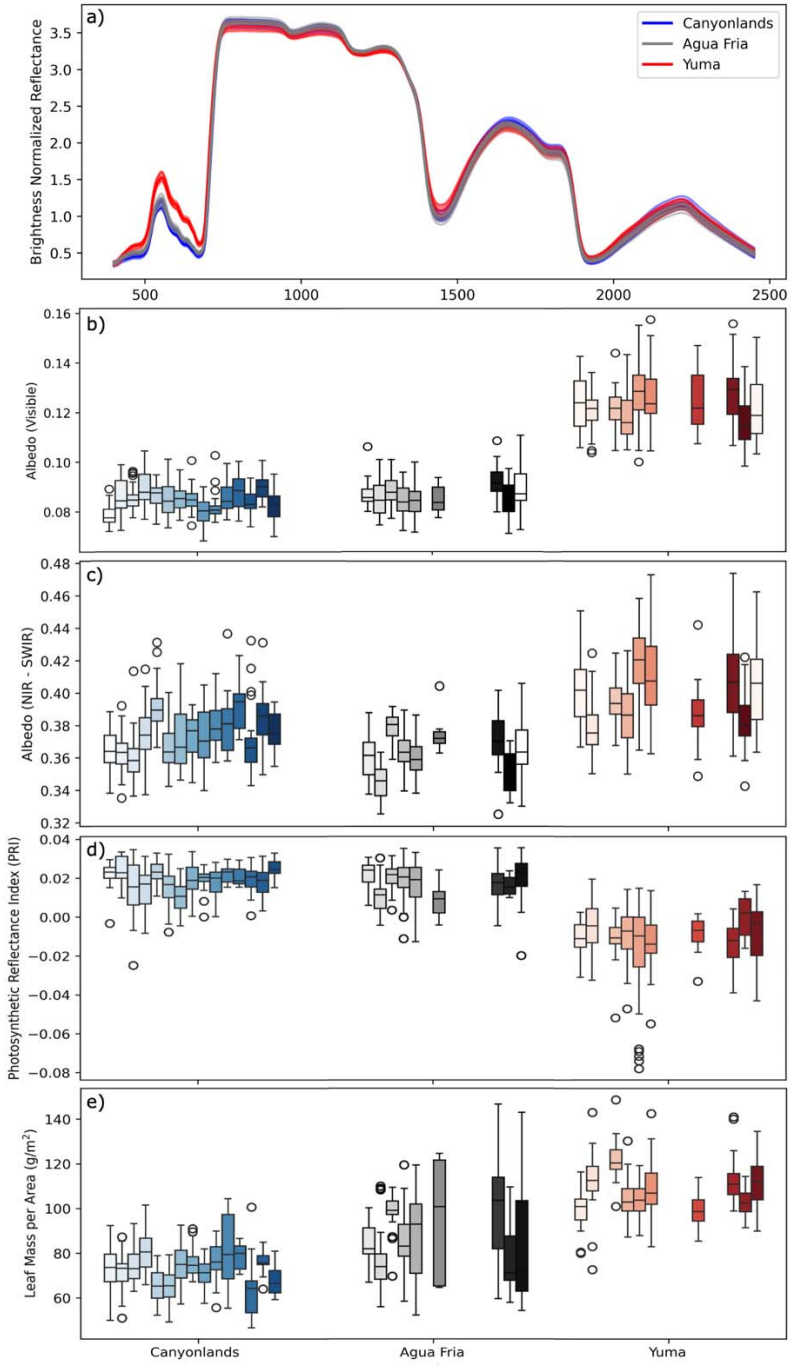
a)
Canyonlands
Agua Fria
Yuma
Brightness Normalized Reflectance
b)
Albedo (Visible)
c)
Albedo (NIR - SWIR)
d)
Photosynthetic Reflectance Index (PRI)
e)
Leaf Mass per Area (g/m²)
Canyonlands
Agua Fria
Yuma

Figure 2

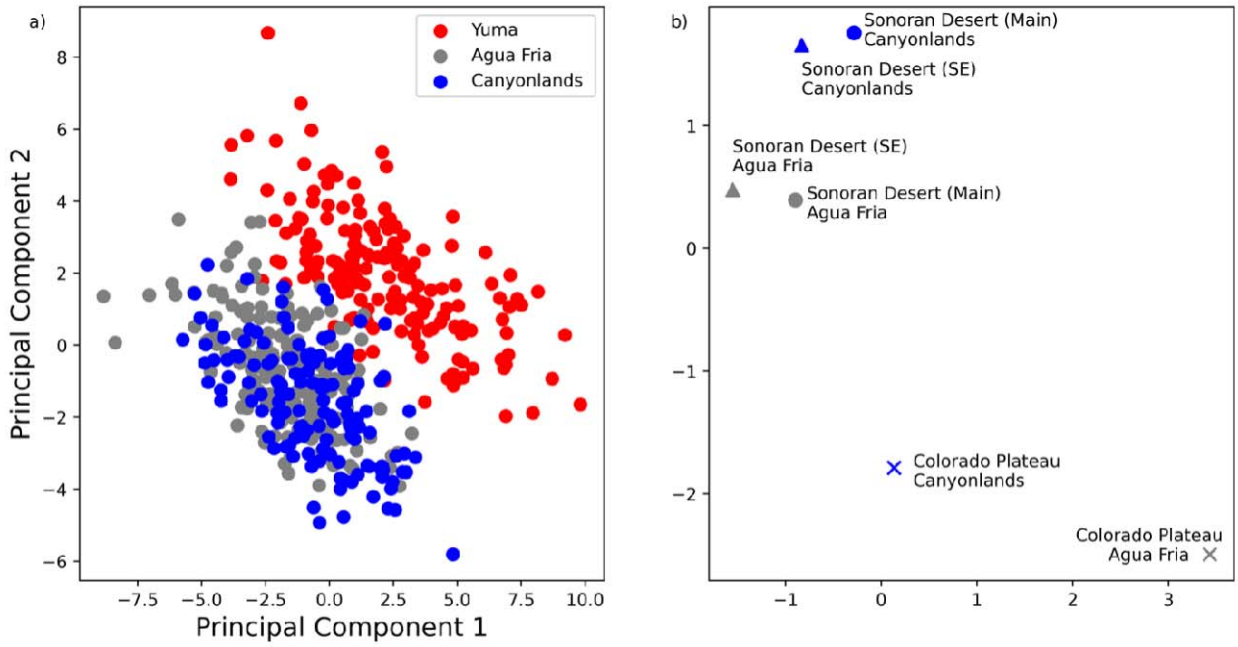
a)
Yuma
Agua Fria
Canyonlands
Principal Component 2
Principal Component 1
b)
Sonoran Desert (Main)
Canyonlands
Sonoran Desert (SE)
Canyonlands
Sonoran Desert (SE)
Agua Fria
Sonoran Desert (Main)
Agua Fria
Colorado Plateau
Canyonlands
Colorado Plateau
Agua Fria

Figure 3

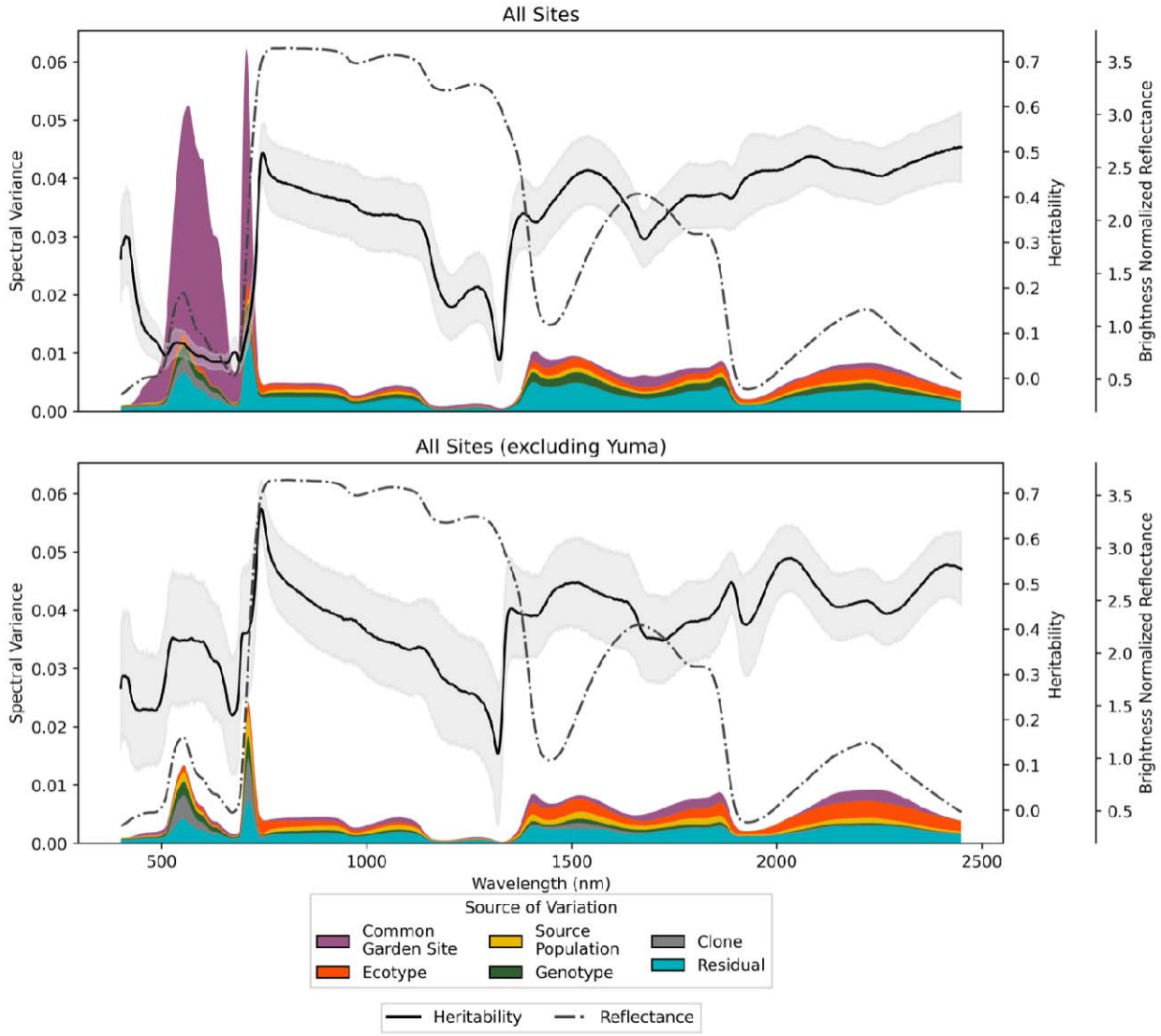
All Sites
All Sites (excluding Yuma)
Spectral Variance
Heritability
Brightness Normalized Reflectance
Wavelength (nm)
Source of Variation
Common Garden Site
Ecotype
Source Population
Genotype
Clone
Residual
Heritability
Reflectance

Figure 4

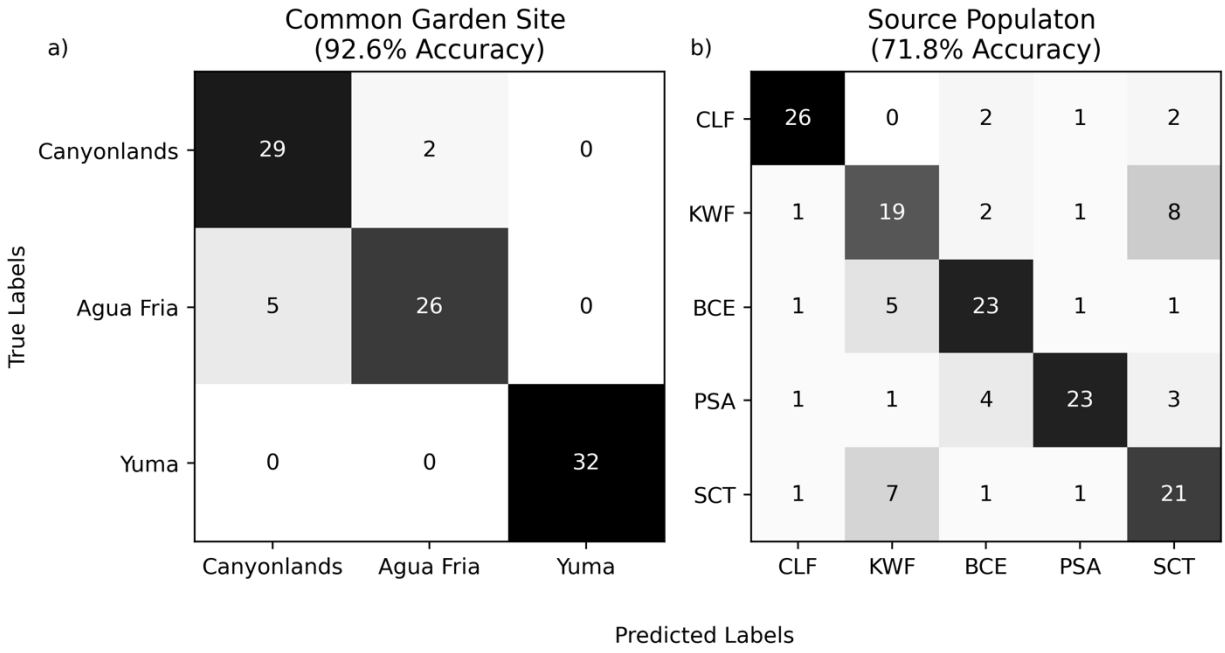
a)
Common Garden Site
(92.6% Accuracy)
Canyonlands
Agua Fria
Yuma
True Labels
29
2
0
5
26
0
0
0
32
Canyonlands
Agua Fria
Yuma
b)
Source Populaton
(71.8% Accuracy)
CLF
KWF
BCE
PSA
SCT
26
0
2
1
2
1
19
2
1
8
1
5
23
1
1
1
1
4
23
3
1
7
1
1
21
CLF
KWF
BCE
PSA
SCT
Predicted Labels

Figure 5